Journal of Colloid and Interface Science 607 (2022) 1050–1060

Contents lists available at ScienceDirect

Journal of Colloid and Interface Science

journal homepage: www.elsevier.com/locate/jcis

Multiple phase transitions and microstructural rearrangements shape milk fat crystal networks

Naomi Arita-Merino [a,b], Laura te Nijenhuis [a], Hein van Valenberg [b], Elke Scholten [a,*]

[a] Physics and Physical Chemistry of Foods, Wageningen University, Bornse Weilanden 9, Wageningen 6700 AA, the Netherlands
[b] Dairy Science and Technology, Food Quality and Design, Wageningen University, Bornse Weilanden 9, Wageningen 6700 AA, the Netherlands

GRAPHICAL ABSTRACT

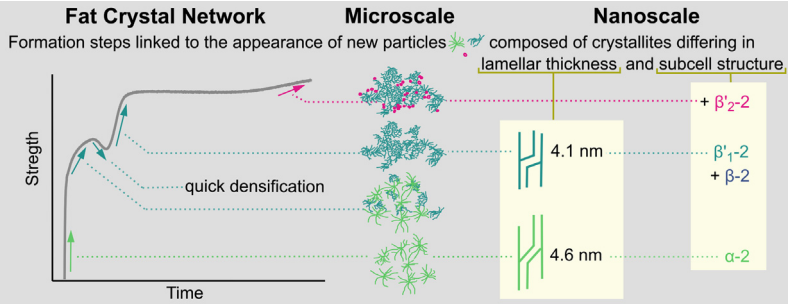

ARTICLE INFO

Article history:
Received 22 July 2021
Revised 12 September 2021
Accepted 13 September 2021
Available online 20 September 2021

Keywords:
Crystallization
Milk fat
X-ray diffraction (XRD)
Microstructure
Phase transition
Polymorphism
Crystal network

ABSTRACT

Hypothesis: The rheology of milk fat, which is strongly related to its functionality, reflects multiscale structural transitions in the colloidal network formed by crystallizing triacylglycerols. Experiments: To relate rheology to structure, early stages of milk fat crystallization at 15–22 °C were studied combining different techniques; XRD and microscopy to study structural changes, NMR to quantify the different structures, and rheology to evaluate their effect on macroscopic properties. Findings: Network strength increased with the synchronized formation of micro- and nanostructures. A rheological response was only obtained when these structures became visibly connected on a microscale, and internal transitional changes could be detected with rheology. On the nanoscale, transitions were linked to the formation of specific crystal polymorphs. We quantified the formation of polymorphs commonly found in milk fat (α-2 and β'_1-2) and of two less commonly obtained polymorphs: β-2 and β'_2-2. For the first time, the formation of these polymorphs was quantified and related to the composition of fat. Besides providing insights into the complex phase behavior of milk fat, this study shows that the structural transitions involved can be characterized and quantified by combining XRD with NMR and be detected at an early stage using rheology and microscopy.

© 2021 The Author(s). Published by Elsevier Inc. This is an open access article under the CC BY license (http://creativecommons.org/licenses/by/4.0/).

1. Introduction

The rheological properties of milk fat (MF) are the result of a multiscale structured network, which has a great impact on the functionality and sensory attributes of several products. In fat crystal networks, there is a hierarchical arrangement that starts with their composing triacylglycerols (TAGs) stacking on top of each other and laterally packing into lamellae; lamellae then epitaxially stack into nanoplatelets that aggregate forming crystallites; crystallites further cluster to form microscopic polycrystalline particles that, in turn, aggregate giving rise to a 3-dimensional network [1].

* Corresponding author.
E-mail address: elke.scholten@wur.nl (E. Scholten).

https://doi.org/10.1016/j.jcis.2021.09.071
0021-9797/© 2021 The Author(s). Published by Elsevier Inc.
This is an open access article under the CC BY license (http://creativecommons.org/licenses/by/4.0/).

The formation of such a complex network is affected by crystallization conditions and composition. MF is composed of at least 3454 different TAG species that vary in molecular weight, degree of unsaturation, and fatty acid (FA) composition [2]. Due to this TAG diversity, liquid and multiple crystalline phases coexist in MF over a wide temperature range (−40 °C to 40 °C) [3].

These crystalline phases in MF can be formed by different structures, referred to as polymorphs. TAG polymorphs can differ both in lateral and longitudinal packing mode (i.e. subcell structure and lamellar thickness, respectively). MF crystalline phases commonly display a lamellar thickness corresponding to the length of two aliphatic chains (2L), and at low temperatures (below ~13 °C), thickness corresponding to three aliphatic chains (3L) can also be observed [4–6].

The most common subcell structures are α, β' and β polymorphs, listed in increasing order of stability, density and melting point [7]. A polymorphic phase can be designated by the type of lateral and longitudinal packing (e.g. α-2 for an α phase with lamellar thickness of two aliphatic chains). MF commonly crystallizes into a stable β'-2 phase. At temperatures below ~20 °C, a metastable α phase forms first and subsequently transitions into a more stable β' phase [8]. At temperatures between the clear points of α and β' (~20–35 °C), β' directly forms from the melt and no α is observed [8]. The occurrence of a β phase in MF has been somewhat controversial, as it has been intermittently reported in literature and its quantification based on wide angle X-ray diffraction patterns (WAXD) has only recently been achieved [9]. While other polymorphs may be formed, α and β' are the most common and abundant ones. The formation of these two polymorphic phases has been linked to a stepwise crystallization process.

Herrera et al. [10] studied the crystallization of MF under isothermal conditions. They reported a one-step crystallization at temperatures above 25 °C, whereas a two-step process was observed at lower temperatures [10]. In that study, the crystallization processes were monitored trough changes in the solid fat content (SFC). However, this study did not provide information on the development of the fat crystal network. The evolution of the crystallization process can be further assessed by measuring the changes in the rheological properties, which provides additional information on the organization of the structuring elements within the network.

Rheology has been used to study the kinetics of fat crystallization together with complementary techniques [11–13], finding good agreement between the transitions identified and the rheological changes observed. Specifically for MF, Wiking et al. [13] studied the effect of different cooling rates using small amplitude oscillatory shear (SAOS) tests in combination with other techniques. They observed the development of the network in one or two steps when cooled at 0.1 °C min^{-1} or at 10 °C min^{-1}, respectively [13]. Linked to those rheological changes, they recorded an equivalent number of crystallization events using differential scanning calorimetry (DSC) and similar evolutions in the SFC [13]. Using X-ray diffraction (XRD), they confirmed that the two-step process was related to the formation of α-2 polymorph and its transition into β'-2, while the microscopy images revealed the formation of two different microstructures for the different processes [13]. Their study exemplifies the potential of SAOS in combination with other techniques to monitor the formation of fat crystal networks and elucidate the structural changes involved.

Following a similar approach, we further explored the relation between multiscale structural changes and the evolution of the rheological properties of MF networks during crystallization, combining SAOS, nuclear magnetic resonance (NMR), light microscopy and XRD. We aimed to expand our knowledge on the effect of temperature on the isothermal crystallization of MF, linking the macroscopic rheological properties of the network to the microstructure and the composing crystalline phases. In contrast to previous studies, we investigated the effect of temperature in more detail and applied our recently published method [9] to quantify the different polymorphic phases. With this approach, we showed that structural transitions beyond the known one- and two-step processes occur under specific conditions, and we were able to study the formation of less common structures, such as the β polymorph, in a quantitative manner.

2. Experimental section

Anhydrous milk fat (AMF) was kindly provided by FrieslandCampina (The Netherlands). Detailed TAG and FA profiles of this sample can be found elsewhere [14]. The isothermal crystallization of AMF was studied by monitoring the evolution of rheological properties, solid fat content (SFC), polymorphism, and microstructure morphology. Seven crystallization temperatures (15, 16, 17, 18, 19, and 22 °C) were used to study the effect of temperature. A cooling rate of 5 °C min^{-1} was used for all the experiments. This rate was suitable for all the experimental techniques used and was fast enough to avoid crystallization during the cooling step.

2.1. Rheological properties

Small amplitude oscillatory shear (SAOS) experiments were performed on a stress-controlled rheometer (MCR 502, Anton Paar) using a concentric cylinder geometry (CC10 TI-SN3944, Anton Paar). 1 ml of melted AMF was loaded in the cell and was kept at 65 °C for 1 h to clear the crystal memory. Then, the sample was cooled at 5 °C min^{-1} to one of the crystallization temperatures. Once the target temperature was reached, the evolution in storage modulus (G′) was followed during 2 h of isothermal crystallization. To ensure that the measurements were carried out within the linear viscoelastic region, low strain (0.01%) and frequency (1 Hz) were selected. G′ values were recorded every 5 s to monitor the network formation closely, while providing enough time for the shear to develop in the entire shear gap. To avoid possible effects of fat fractionation, no consecutive measurements were carried out using the same aliquot. The experiments were conducted in triplicate.

2.2. Solid fat content

A low-resolution nuclear magnetic resonance (NMR) spectrometer (Minispec mq20, Bruker) was used to measure the SFC. The SFC determination is based on the difference in magnetization decay rate for hydrogen atoms in a liquid and in a solid phase, after applying a pulsed magnetic field. The solid to liquid ratio can be calculated from an NMR magnetization decay curve. SFC values were determined according to the AOCS method Cd 16b-93 [15], although the thermal treatment was different. An NMR tube was filled with 2 ml of melted fat and was kept at 65 °C for 1 hour to clear the crystal memory. Then, using external water baths, the sample was cooled at 5 °C min^{-1} to one of the crystallization temperatures. Upon reaching the target temperature, the tube was placed in the spectrometer and SFC values were recorded continuously (every ~10 s) for 2 h, while the measuring cell was kept at the crystallization temperature. Measurements were performed in duplicate.

2.3. Polymorph formation

Changes in polymorphism were studied using wide angle X-ray diffraction (WAXD) and small angle X-ray diffraction (SAXD).

Diffraction patterns were collected using a powder X-ray diffractometer (D8 Advance, Bruker) with a Cu anode (Kα λ 0.15406 nm). The diffractometer was operated at 40.0 kV and 40.0 mA in Bragg-Brentano geometry using a divergence slit of 0.6 mm and a detector opening of 2.914°. In all the measurements, we used a temperature control chamber (TTK600, Anton Paar) equipped with a standard sample holder for powder XRD in reflection geometry. The pretempered sample holder was filled with ~ 140 μl of melted AMF and kept for 10 min at 65 °C to clear the crystal memory. The sample was then cooled to one of the crystallization temperatures at 5 °C min^{-1}. Once the temperature was reached, continuous scans were acquired for 2 h at constant temperature. WAXD scans were recorded over a 15–30° 2θ angle region (10.6-21.1 nm^{-1} in reciprocal lattice spacing q) in 0.02° steps, taking 0.1 s per step. SAXD scans were recorded over a 0.8–8° 2θ region (q 0.57–5.7 nm^{-1}) in 0.02° steps, taking 0.3 s per step. For interpretation of the results, 2θ values were converted to q or d-spacings d according to $d = 2\pi q^{-1} = n\lambda(2\sin\theta)^{-1}$, where n is 1 and λ is the X-ray wavelength.

2.4. Quantitative phase analysis

The time-resolved diffraction patterns were qualitatively analyzed, identifying the different crystalline phases based on the diffraction peaks observed. Phases with different lamellar thickness were identified based on the d-spacings of the first order diffraction peaks in the SAXD patterns. The different subcell structures were identified according to the long established classification [16] using characteristic d-spacings reported for MF [17–19]. The relative contribution of the identified phases was quantified using a method described by us previously [9]. This method was originally proposed for WAXD data, and we extended its use for SAXD data. In short, the WAXD and SAXD patterns, in terms of intensities as a function of q, were decomposed following a "peak by peak" approach. A model composed of Pearson VII functions was fitted to each background subtracted pattern. According to the phases identified in the qualitative analysis, a Pearson VII function was centered around the observed maximum of each peak, using fitting parameters that define the shape, height and width. In the case of the WAXD patterns, the broad liquid peak was also fitted with a Pearson VII function. To quantify the area contribution to the diffraction pattern of each phase (polymorph), the obtained functions for the respective phases were integrated and added up. The total diffraction area of each phase was related to its respective mass fraction using a phase-specific response factor. A response factor was experimentally derived for every crystalline phase and for every WAXD and SAXD measurement. The use of these factors accounts for structural differences among phases and for any instrumental effect. These response factors were obtained using the time-resolved SFC results, by nonlinear least-squares optimization of an adaptation of the Hill and Howard relation as described previously [9]. More details on the approach can be found in our previous work [9].

2.5. Synchrotron X-ray scattering

We studied the crystallization of AMF at 17 °C in more detail, and the consecutive melting of the crystalline phases during heating at 5 °C min^{-1}. Synchrotron radiation wide-angle X-ray scattering (WAXS) and small-angle X-ray scattering (SAXS) analyses were performed on the beamline BM26B at the European Synchrotron Radiation Facility (ESRF) in Grenoble (France). WAXS and SAXS patterns were simultaneously and continuously collected every 16.4 s in the 10.6–21.1 nm^{-1} and 0.5-4 nm^{-1} q regions, respectively. After being corrected for the detector response and normalized by the primary beam intensity, the 2-dimensional patterns were azimuthally averaged. These patterns were further analyzed as previously described for the XRD patterns.

2.6. Microscopy

The microstructural changes during crystallization were studied using microscopy. Initially, polarized light microscopy was used to confirm the presence of crystals, but could not be used to visualize clear differences in the morphology. Instead, light microscopy was used to visualize the morphology of the crystals. A light microscope (Zeiss Axioskop 2 Plus, Carl Zeiss) equipped with a hot-stage (T95, Linkam). A small aliquot (~2 μl) of melted fat was deposited on a glass slide and covered with a glass cover slip, both preheated at 65 °C. The sample was kept at 65 °C for 10 min before cooling it to the crystallization temperature at 5 °C min^{-1}. Images were taken every 60 s for 2 h to follow the microstructural development during crystallization. After the crystallization period, micrographs were taken during heating at ~2 °C min^{-1} at 1 °C intervals. The experiments were conducted in duplicate, and representative micrographs are reported.

3. Results and discussion

For this study, we selected an industrial sample of AMF. The AMF used displayed the characteristic composition of MF obtained in winter. In comparison with MFs collected in summer [20], this AMF presented relatively high levels of saturated FA (71%), a high level of low- and medium-molecular weight TAGs (23% TAGs with carbon number [CN] of 26-36 and 55% CN38-CN48), and a relatively low level of high-molecular weight TAGs (22% CN50-54) [14].

3.1. Rheological assessment of the network formation

To study the network formation during isothermal crystallization, we measured the changes in the viscoelastic properties at different temperatures ranging from 15 to 22 °C. As the elastic (solid-like) portion of the viscoelastic behavior quickly dominated over the viscous (liquid-like) response, we selected the storage modulus (G′) to characterize the network formation and evolution during crystallization. The network strength, here measured by G′, evolved in a stepwise fashion. For clarity, we classified these steps in four regions (I-IV) as shown in Fig. 1a. Fig. 1 also includes additional results to facilitate their comparison, which will be discussed at a later stage. Additional plots showing G′ and the loss modulus (G″) can be found in the supplementary information (Fig. S1).

During the first hour, at 19–22 °C, G′ increased in one step (region III) followed by a plateau. At lower temperatures, G′ increased in three steps (regions I-III). Additionally, at 17 °C, G′ decreased temporarily, between the G′ increments recorded in regions II and III. At and below this temperature (15–17 °C), an additional increase in G′ was observed in region IV, indicating a fourth step in the crystallization process. As mentioned previously, the stepwise crystallization of MF has been reported before, but only one- and two-step processes have been described in literature [10,12,13]. These results show that the crystallization process in AMF is more complex than previously reported. To elucidate the cause behind the diversity in the G′ evolutions we observed, we further studied these crystallization processes.

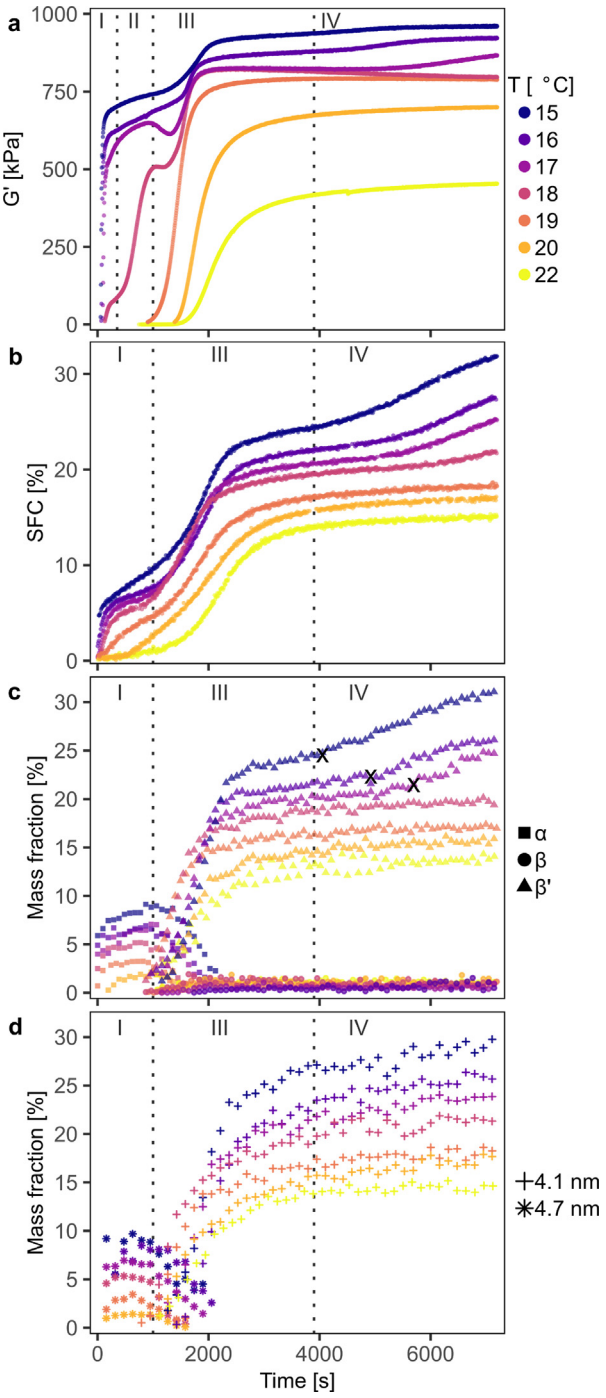

Fig. 1. Synchronized changes in milk fat crystallizing at different temperatures (15–22 °C). Network formation measured as the storage modulus G′ (a), SFC evolution as obtained by NMR (b), evolution of polymorphic phases displaying different subcell structures (c) and different lamellar thickness (d), as quantified from WAXD and SAXD time-resolved patterns, respectively. I-IV indicate different transition regions. The **x** marks the point at which an additional β' peak appeared in the WAXD patterns. One replicate is presented as little variation was observed between replicates.

3.2. SFC evolution

To investigate if the changes observed in the G′ could be directly explained by changes in the amount of matter forming the network, we measured the SFC during the same time frame. Resembling the G′ evolution, the SFC increased in multiple steps (Fig. 1b), thus, we classified the SFC steps in an analogous way as we did for the G′ steps. During the first hour at the highest temperature (22 °C), the SFC increased in one step (III), while it occurred in two steps at all the other temperatures (I and III). As we did not observe intermediate SFC changes between steps I and III, no step II was assigned in Fig. 1b. During the second hour, an additional SFC increment was observed at 15–17 °C and to a much smaller extent for 18 °C (IV). By comparing the evolution in the rheological behavior and the SFC, it is clear that the transitions are synchronized.

The main network strengthening events (i.e. those occurring in regions I, III and IV) coincided with increments in the amount of crystallized fat (SFC). In region III, increments in G′ and SFC coincided at all temperatures. This was also observed for regions I and IV, but with some exceptions at higher temperatures. At 19 and 20 °C in region I and at 18 °C in region IV, there were small SFC increments (2–4%), but no changes in G′ were recorded. Aside from these minor discrepancies, which will be further discussed in terms of the network structure, SFC changes were reflected in G′ changes, verifying that both techniques can provide information on the crystallization and network formation of MF.

Although, in general, G′ increments could be attributed to SFC increments, this was not the case for all G′ changes. The occurrence of multi-step G′ evolutions, more evident at 16–18 °C, could not be explained by changes in SFC, which increased in only two steps during the first hour. In particular, it is clear that the G′ decrease recorded at 17 °C did not correspond to a reduction in the SFC. This shows that rheological data provides additional information on the fat network formation. As the rheological properties of a network result from the interactions between the solid fat particles, G′ is largely determined by the SFC, but additional structural parameters also play a role. These additional changes in G′ thus reflect structural changes within the crystal network. We studied these structural changes by investigating the microstructure and the underlying arrangement of TAGs in the crystalline structures.

3.3. Identification and characterization of the crystalline phases

To interpret the changes in the rheological properties, we studied the structural changes in the crystals forming the network. As discussed, TAGs self-assemble in different crystalline structures (polymorphs) that can be characterized with XRD. We used time-resolved XRD to study the evolution of the crystalline phases, characterizing the changes in the lateral packing of TAGs by WAXD and in their longitudinal stacking into lamellae by SAXD.

To visualize the structural transitions, we used the time-resolved patterns to produce heat maps where the color changes show the intensity changes of the peaks at the different q ranges over time. The heat maps in Fig. 2 reflect the changes in the WAXD and SAXD patterns recorded at representative temperatures (15, 17 and 22 °C). For clarity, examples of individual patterns that were used to create the heat maps were included. As can be seen in Fig. 2, there was a synchronized appearance and disappearance of WAXD and SAXD peaks, showing how the phase transitions involved changes in both the lateral and the longitudinal arrangement of TAGs. Thus, we identified the different polymorphs according to the type of subcell and lamellar structure.

In the WAXD patterns, we identified three sub-cell structures; we attributed apparent maxima at ~0.415 nm to α, ~0.42 nm and ~0.38 nm to β' and ~0.46 nm to β-polymorphs, as reported in literature [17–19]. In addition to the crystalline peaks, a broad ~0.45 nm peak was attributed to a liquid phase. In the SAXD patterns, we linked the position of the most intense peaks (first order diffraction peaks L_{001}) to the thickness of the lamellae. We observed peaks centered around two d-spacings: ~4.7 nm synced with the α patterns and ~4.1 nm synced with β' and β patterns.

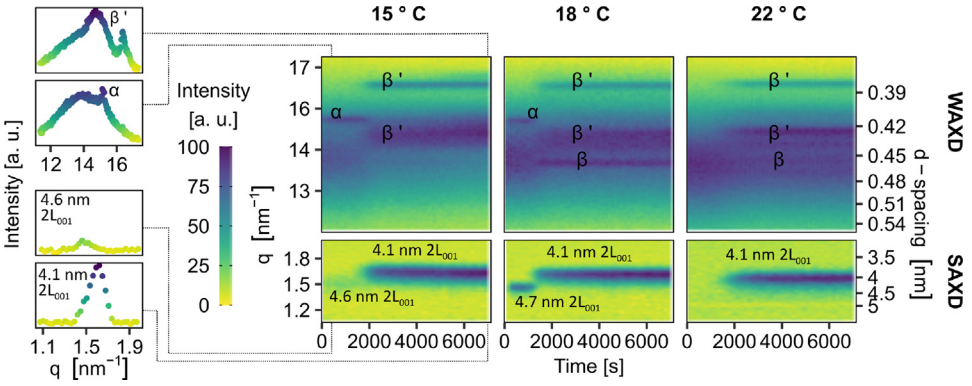

Fig. 2. Time-resolved WAXD and SAXD patterns of anhydrous milk fat crystallizing at representative temperatures. Examples of individual patterns recorded at 15 °C are included with guides to their corresponding time points in the heatmap. The color scale corresponds to the intensity in arbitrary units (a. u.), normalized separately for WAXD and SAXD experiments per temperature.

Both types of peaks correspond to lamellae with the length of two aliphatic chains (2L). At all temperatures at which both β' and β phases formed, only one L_{001} SAXD peak was detected, as is common for MF [18,21]. Depending on the temperature, we identified the formation of different polymorphs: β'-2 was observed at all temperatures, α-2 at 15–20 °C and β-2 at 16–20 °C. Before discussing these results further and identifying specific polymorphic transitions, we quantitatively analyzed the XRD data to be able to relate their transitions to the rheological evolutions.

To characterize and later quantify the crystalline phases, we decomposed the diffraction patterns to separate the contribution of each phase at the different temperatures. As illustrated in Fig. 3 for 16 °C and described in the methods section and in further detail in our previous work [9], the background subtracted patterns were decomposed fitting each peak with a Pearson VII function by nonlinear least-squares optimization. Using the decomposition of the SAXD patterns, we determined the lamellar thickness (long spacings) with precision from the center of the L_{001} peaks (Table 1). In agreement with literature [18], there was a tendency for the formation of thicker lamellae with increasing temperatures. For example, for the α-2 phase, we observed a thickness of 4.550 ± 0.049 nm at 15 °C and a greater thickness of 4.706 ± 0.014 nm at 20 °C. For the β'-2 and the β-2 phases, the lamellar thickness

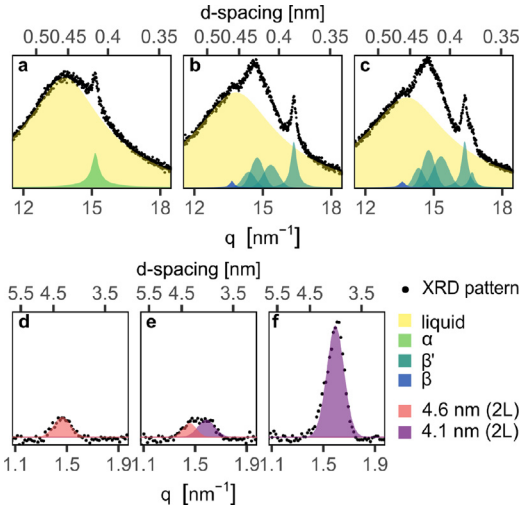

Fig. 3. Decomposition of representative XRD patterns recorded at 16 °C. WAXD patterns before the polymorphic transition (a), after the polymorphic transition (b) and after an additional β' peak appeared at 0.376 nm (c). SAXD patterns before (d), during (e) and after the polymorphic transition (f).

Table 1
Lamellar thickness of the polymorphic phases formed at different crystallization temperatures (T).

T [°C]	α 2L [nm]	β' and β 2L [nm]
15	4.550 ± 0.049	4.063 ± 0.016*
16	4.632 ± 0.012	4.087 ± 0.006
17	4.639 ± 0.055	4.093 ± 0.004
18	4.683 ± 0.008	4.095 ± 0.003
19	4.688 ± 0.009	4.106 ± 0.004
20	4.706 ± 0.014	4.117 ± 0.003
22	-	4.146 ± 0.025

* The value at 15 °C corresponds to a β' 2L phase.

increased from 4.087 ± 0.006 nm at 16 °C to 4.146 ± 0.025 nm at 22 °C. As suggested by Mazzanti et al. [18], this could be the result of smaller TAGs being able to crystallize at lower temperatures and forming thinner lamellae.

While the decomposition of the SAXD patterns provided more information about the thickness of the lamellae, the decomposition of the WAXD patterns allowed us to determine the short spacings of the different polymorphs, which correspond to the distances between the aliphatic chains in the lamellae (Table 2). In Fig. 3, the decomposition of representative WAXD patterns is illustrated for scans displaying crystalline contribution from α polymorph only (a) and from β' and β polymorphs (b). As is typically described for MF [17–19], β' polymorph was characterized by two apparent maxima only (~0.42 nm and ~0.38 nm) (Fig. 2). However, as we previously reported for AMF [9], four peaks (0.437, 0.425, 0.409, 0.384 nm) were required to consistently and accurately decompose the patterns including β'. During the second hour at temperatures below 18 °C, the WAXD pattern decomposition revealed the appearance of an additional peak corresponding to a spacing of 0.376 nm (Fig. 3c). As the area of this peak increased simultaneously with the area of the four β' WAXD peaks and the corresponding 2L SAXD peak, we assigned this peak to a β'-2 phase as well.

Table 2
d-spacings of the polymorphs formed in anhydrous milk fat.

α [nm]	β' [nm]	β [nm]
0.415 ± 0.001	0.437 ± 0.004	0.459 ± 0.001
	0.425 ± 0.005	
	0.409 ± 0.003	
	0.384 ± 0.001	
	0.376 ± 0.001*	

* Associated with a second β' phase observed in the second hour of crystallization at 15–17 °C.

The nature of this second β'-2 phase is further discussed in Section 3.5.2. In addition to the characterization of the crystalline phases, the XRD pattern decomposition also allowed us to quantify the different crystalline phases.

3.4. Quantitative phase analysis

To quantify the evolution of the different crystalline phases over time, we used the pattern decomposition to identify the area contribution of each phase to the diffraction pattern. We converted these areas to their respective mass fractions using phase-specific response factors derived from the SFC data, as described in [9] and illustrated in Fig. 4. This allowed us to quantify the evolution of crystalline phases with different lateral (Fig. 1c) and longitudinal packing modes (Fig. 1d) at all the studied temperatures.

The quantitative phase analysis (QPA) revealed clear similarities between the transitions in the subcell structure and lamellar thickness, and the changes in G′ and SFC (Fig. 1). The regions identified for the SFC increments and the main G′ increments (I, III and IV) coincided with the formation of different crystalline phases. At 22 °C, no α-2 formation was observed, but only β' and β phases. At temperatures below 22 °C, first an α-2 phase was formed in region I at the beginning of the isothermal period. In step III, β' and β phases were formed at 16–22°C, while only β formation was observed at 15 °C. As only one 2L peak was recorded, we assume that both β and β' phases had a similar lamellar thickness.

Thus, we were able to unequivocally link the one-step SFC formation at 22 °C to the direct crystallization of liquid TAGs into stable crystalline phases (β'-2 and β-2), and the two-step SFC formations at lower temperatures to the formation of β'-2 and β-2 phases, mediated by the initial formation of a metastable α-2 phase. This is in agreement with the study of [8], who reported for AMF the formation of β' directly from the melt at 20 °C but mediated by α at lower temperatures. In our study, we could also quantify these different polymorphs. As expected, lower temperatures resulted in more abundant α-2 and β'-2 phases, as more TAG species reach a supercooled state. Interestingly, the amount of β-2 polymorph was not affected in the same way by temperature.

At 17–22 °C, a constant amount (~1%) of a β-2 formed at the same time as the β'-2 phase (~1000 s). In contrast, at 16 °C, β-2 formed 772 s later than β'-2 and reached a slightly lower level (0.6%). At a lower temperature of 15 °C, no β-2 could be detected. Thus, a β-2 phase formed only at lower extent of supercooling, i.e. slower crystallization. Several studies have suggested that a considerable amount of liquid fat is required for the formation of β polymorphs in milk fat [3,22–24]. The need for an abundant liquid phase for β crystals to form is in agreement with our results, as the formation of β-2 was inhibited at lower temperatures. At low temperatures, the SFC levels were already high from the beginning of the isothermal period, which would increase the viscosity and thus present a kinetic constraint for β-2 crystals to form. Although the formation of β-2 was expected, a more unexpected effect was the simultaneous formation of β-2 and β'-2 at 17–22 °C. As TAGs crystallize faster into less stable polymorphs ($\alpha < \beta' < \beta$ in increasing order of stability and Gibbs free energy) [22], the β-2 phase would be expected to consistently form after the β'-2 formation, in a similar way that β'-2 forms after the initial α-2 formation.

Another interesting observation was the appearance and growth of the additional (0.376 nm) peak during the second hour at temperatures below 18 °C (marked by an **x** in Fig. 1c), linked to SFC and G′ increments (IV). This change was clearly reflected in the phase quantification based on WAXD patterns, while the quantification based on SAXD patterns only showed a minor increment. As already discussed, we attributed this peak to a β'-2 phase, but we could not determine whether it was the result of a new crystalline phase or the growth of the original β'-2 phase, as both events could produce an additional apparent maximum. The QPA results support the idea of a new β'-2 phase, as it clearly links the growth of the (0.376 nm) peak to a separate crystallization event.

Although the quantitative analysis provided a clearer picture of certain crystallization events, it could not provide a full explanation regarding the formation of β-2 together with the β'-2 phase, and the appearance of an additional β' peak. Moreover, it also did not explain all the rheological changes recorded at intermediate temperatures. In the region in which an additional G′ increment was recorded (II), we only observed a plateauing of the α-2 phase, and therefore we could not attribute the rheological changes to transitions in either the lateral or the longitudinal packing mode of the TAGs, nor specific changes in the amount of the crystalline phases. Furthermore, the decline in G′ observed at 17 °C could not be attributed to a decrease in SFC or a polymorphic transition. Acknowledging the limitations of a lab-scale diffractometer, we further investigated these observations using synchrotron radiation.

3.5. Synchrotron XRD

We repeated one of the lab-scale XRD experiments using synchrotron radiation to verify and study in detail our previous findings. We selected 17 °C to study the formation of all the polymorphs previously observed and the rheological events in regions II and III. To follow the delayed formation of the additional β' peak more closely, we extended the isothermal period to 3 h. In addition, we studied the melting behavior of the different phases formed.

The synchrotron WAXS and SAXS patterns of AMF at 17 °C (Fig. 5), recorded simultaneously, displayed the same transitions

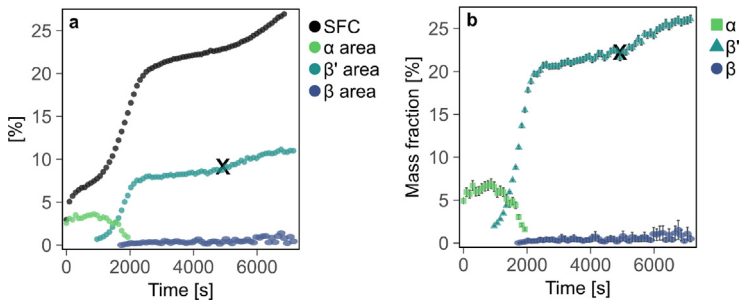

Fig. 4. Quantitative phase analysis of anhydrous milk fat crystallizing at 16 °C. Area contribution to the WAXD patterns of each crystalline phase and SFC by NMR (a), used to calculate the mass fraction of the different phases over time (b). The error bars correspond to the 95% confidence interval. As the error margins are small, they become nonvisible in most cases. The **x** marks the point at which an additional β' peak appeared in the patterns.

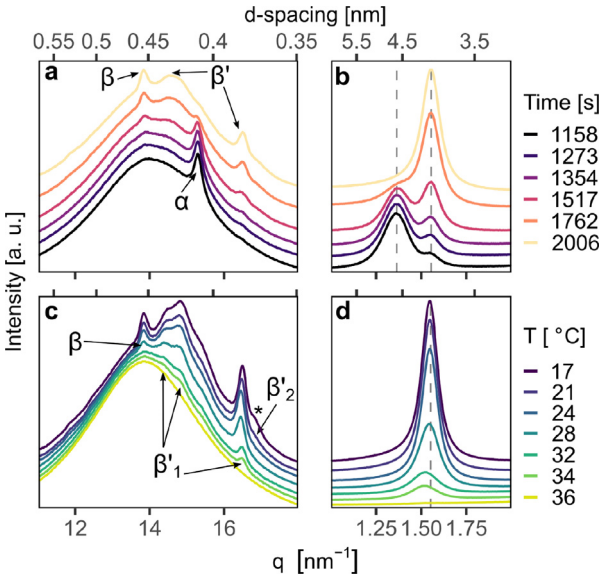

Fig. 5. Synchrotron WAXS (a and c) and SAXS patterns (b and d) of anhydrous milk fat recorded during the polymorphic transition at 17 °C (a and b) and during melting of the formed crystals (c and d). The * marks an additional peak observed during the second hour, attributed to β'_2-2 polymorph. The arows point to the characteristic peaks per polymorph recorded at the highest temperature at which they could be clearly distinguished.

as our lab-scale results. These results confirm 1) the formation of the α-2 phase from the melt in region I, 2) the simultaneous formation of the β'-2 and β-2 phases and disappearance of α-2 in region III, and 3) the appearance of a 0.376 nm peak alongside the growth of the other β'-2 peaks in region IV. The patterns recorded in region IV, and until the end of the crystallization time (patterns in Fig. 5c and d), displayed peaks corresponding to the formation of a β phase and possibly to two different β' phases, but only one 2L long spacing. To gain more information about these crystalline phases, we studied their melting behavior.

From the WAXS patterns recorded during heating, we determined the melting ranges for the different peaks, considering the temperatures at which the peaks started to shrink and the temperatures at which they could not be clearly distinguished anymore. We recorded three melting ranges for the different WAXS peaks (Fig. 5c): 20–24 °C for the 0.376 nm β' peak, 24–29 °C for the β peak and 20–36 °C for the other four β' peaks. At the same time, the SAXS peak continuously declined, but its apparent maximum shifted slightly towards longer spacings at temperatures above 29 °C (Fig. 5d). The separate melting ranges confirm the formation of three separate stable crystalline phases with similar lamellar thickness: a typical β'-2 phase that forms together with a lower melting β-2 phase, and a low melting β'-2 that forms during the second hour. The two β'-2 phases can be considered as two separate β'-2 polymorphs with different origins. Combining these observations with the quantification of the different polymorphs, we can now elaborate on the formation of the less commonly observed polymorphic phases.

3.5.1. Simultaneous formation of β′-2 and a lower melting β-2 phase

Within the first 2000 s at 17–22 °C, ~1% of a β-2 phase formed at the same time as the predominant β'-2 phase. This β-2 phase completely melted at a lower temperature (29 °C) than the β'-2 phase (36 °C). These observations can be explained only if these two phases are formed by different TAG groups. If the same group of TAGs would form both polymorphs, their crystallization would first lead to the formation of the less stable polymorph (β'-2) and later to the formation of the more stable polymorph (β-2), given the monotropic nature of TAGs. As this was not observed, it is unlikely that the two phases originate from the same TAG species. Our results provide evidence that a β polymorph is formed in MF by a specific group of TAGs, different from the ones crystallizing into β'. This has been suggested in previous studies based on the simultaneous appearance of β' and β according to lab-scale XRD data [9,23], but could now also be confirmed with the excellent time-resolution of the synchrotron data.

We propose that the β polymorph in AMF can readily form only within a narrow temperature range due to a combination of thermodynamic and kinetic constraints. At temperatures above that range, the β-tending TAGs would remain in the liquid phase as they would not be sufficiently supercooled. At temperatures below that range, although the β-tending TAGs would be in a supercooled state, their crystallization would be impaired by a higher viscosity, as other TAGs would quickly arrange into α crystals, thereby increasing viscosity. This temperature range would be affected by composition and cooling rate.

Mazzanti et al. [18] reported that β polymorph formation in AMF is induced by fast cooling (3 °C min^{-1}) or low crystallization temperatures (17.5 and 20 °C). In their study, they only observed the formation of β when α was formed first, and therefore they suggested that β formation was dependent on the previous amount of α formed. Our results contradict this hypothesis, as we recorded the formation of β-2 at 22 °C without an initial formation of α-2. In addition, at the other temperatures, the amount of β-2 formed was unrelated to the amount of α-2 formed, again indicating that the crystallization of these polymorphs can be independent. Nevertheless, the results of Mazzanti et al. [18] strengthen our hypothesis that a combination of thermodynamic and kinetic constraints is responsible for limiting β formation. In their study, the crystallization onset was delayed by faster cooling rates. As a result, there was a longer period in which β-tending TAGs were sufficiently supercooled and the SFC had not reached levels high enough to impair their movement, allowing β crystals to form. Moreover, they did not observe β formation at higher temperatures (22.5 °C and 25 °C), which can be explained by an insufficient degree of supercooling of the β-tending TAGs.

Our quantitative analysis suggests that the concentration of β-tending TAGs present in MF is low, as the β-2 phase quickly reached the same plateau value (~1%) for all temperatures above 16 °C. A low content of β-tending TAGs, combined with the narrow temperature range in which β can readily form, would explain why the β polymorph is either absent in other studies [8,17], or only present at very low levels [4,18].

Regarding the nature of the β-tending TAGs, one could presume that they contained either shorter or more unsaturated FAs than the main TAG groups composing the β'-2 phase, as our results showed that β-2 had a lower clear point than β'-2 (29 °C vs 36 °C). However, this is not necessarily true, as a β phase coexisting with an abundant β' phase can melt at lower temperatures than the β' phase [7]. Tzompa-Sosa et al. [23] observed that the formation of β polymorph was related to high levels of CN52–54 TAGs. Based on studies with pure TAGs, Timms [7] reported three groups of TAGs that are stable as β-2 polymorph: (1) monoacid TAGs, (2) TAGs in which the FAs differ by 4 or 2 carbon atoms and (3) TAGs containing C18:1 *trans*. Thus, it is likely that the β-tending TAGs in milk fat have a high molecular weight, correspond to one or more of the groups identified by Timms, and are present in a low concentration but that at least account for 1% of the TAGs. Still, according to the latest survey of MF TAGs [2], there is an unknown, but certainly high number of components in milk fat that fulfill these requirements. Although our results demonstrate that specific TAG groups are responsible for the formation of a β polymorph,

further investigation is still needed to determine the nature of those TAGs and if the β polymorph can also form through a polymorphic transition from the α polymorph.

3.5.2. Formation of an additional β'-2 phase

During the second crystallization hour at temperatures below 18 °C, additional G′ and SFC increments were recorded, coinciding with the growth of the β'-2 diffraction peaks and the appearance of an additional β' peak (0.376 nm). These changes were greater and occurred earlier at lower temperature. During heating, this additional β' peak was the first to completely melt (at ~24 °C). As we clearly observed all these changes as separate crystallization and melting events, we attribute them to a separate β'-2 phase rather than to the growth of the first β'-2 phase formed.

To the extent of our knowledge, there are limited studies reporting a similar crystalline phase in MF. Lopez and coauthors [4,5] also reported the formation of different β' phases, as they obtained four apparent maxima (0.378, 0.383, 0.425 and 0.437 nm) for AMF when crystallized at 4 °C for more than 100 h. They assigned the four peaks to two separate β' phases: 0.383 and 0.425 nm peaks to β'_1 and 0.378 nm and 0.437 nm peaks to β'_2. They also reported similar clearing points as the ones we obtained; 37 °C for β'_1 and 23.5 °C for β'_2 [5], which confirms the presence of different β' phases. Based on our results and those published by Lopez et al. [4,5], it is clear that two β' phases can coexist in MF. We thus adopted the same nomenclature. We refer to the second β' phase, formed in region IV at 15-17 °C, and with a clear point of 24 °C as β'_2. Both polymorphs show the same four short spacings (Table 2), but β'_2 shows a distinct additional short spacing at 0.376 nm.

We concluded that the β'_2-2 phase formed from the melt, from a group of TAGs different than those in the β-2 and β'_1-2 phases. We inferred this from the separate SFC increment in region IV and the fact that the β-2 and β'_1-2 diffraction peaks did not decline with the growth of the additional β'_2-2 peak. Thus, it is likely that a separate type of TAGs crystallized into β'_2-2 polymorph in region IV, once their concentration reached supersaturation levels in the liquid phase as the amount of liquid fat decreased considerably in region III. As mixed saturated/unsaturated asymmetrical TAGs are typically β' stable [7], it is expected for the two β'-2 phases to be formed by two groups of asymmetrical TAGs that differ in configuration, chain length or unsaturation level. The lower clearing point of the β'_2-2 phase (~24 °C vs 36 °C for β'_1-2) could be due to smaller or more unsaturated TAGs forming it. However, as for the case of the β-2 polymorph, more research is needed to determine the exact nature of the TAGs forming the β'_2-2 polymorph in MF.

3.6. Visualization of the microstructure

Even with the additional analysis using synchrotron radiation, we could not link the intermediate G′ increment (II) or the G′ decline at 17 °C with a crystallization event or a polymorphic transition. As the changes in G′ were likely to be related to changes in the microstructure of the crystal network, we followed the isothermal crystallization for 2 h at different temperatures using microscopy. Although we observed a variety of microstructures forming and disappearing over time, we could distinguish patterns in the microstructural changes. These changes can be seen in the representative pictures taken at different temperatures during crystallization (Fig. 6). Videos recorded during crystallization can be found in the supplementary information.

At 15–17 °C, we observed the formation of a dense network. Although we could not distinguish the individual elements in these networks, the images suggest the presence of spherulites (Fig. 6 for 17 °C, region I). At 18–22 °C, we observed the formation of spherulites that at some point became numerous and large enough to form a network (Fig. 6 for 19 and 22 °C). In general, with decreasing temperature, we observed denser networks with fewer voids and smaller spherulites. These microstructures evolved differently depending on the temperature, aligned with the changes in G′ and SFC, and with the formation of different polymorphs.

The microstructural evolutions can be summarized in four changes that coincide with the three crystallization events (I, II and IV) and the intermediate rheological change (II). As can be seen in Fig. 6 we observed the appearance of new elements in three regions: the first elements appeared in region I at 15-20 °C (indicated by green circles), new elements appeared in region II at all temperatures (indicated by blue arrows) and a different type of small elements appeared on the edges of the existing structures in region IV at 15-18 °C (indicated by pink circles). In region III, no new elements appeared, despite being the period in which the polymorphic transition took place according to the XRD results. Instead, region III was characterized by the steep growth of the elements formed in region II (arrows in Fig. 6), and by the disappearance of the elements formed in region I (indicated by green circles in Fig. 6). As will be discussed in the following section, the visualization of the microstructural evolution provided the last piece of information needed to explain all the changes in the rheological properties, i.e. G′, and to relate the transitions observed to events at different length scales.

3.7. Multiscale transitions behind stepwise network formations

Combining our results, we elucidated the events behind the G′ evolutions, as is schematically depicted in Fig. 7. At 15–20 °C, coinciding with the SFC increment in region I, liquid TAGs crystallized into α-2 polymorph, forming an initial type of microscopic element. At 15–18 °C, these microscopic elements formed a network, which explains the G′ increments observed. In contrast, at 19 °C and 20 °C, the α-2 crystallites formed individual spherulites without forming a 3D network, which explains why the SFC increased but no G′ increments were observed in that period. At 22 °C, above the clear point of α polymorph, no changes in G′, SFC, micro- and nanostructure were observed.

In region II, at all temperatures, we observed the formation of new microscopic elements. The morphology of these elements clearly differentiated them from the elements formed by the α-2 polymorph in region I. Because of this clear difference with the α-2 elements, we expected that the appearance of the new elements would match the initial detection of β'_1-2 and β-2 polymorphs by XRD. However, β'_1-2 and β-2 polymorphs were not yet detected in region II with XRD, but were consistently detected later (region III). This apparent discrepancy between the detection of the initial structural transitions on the microscale and the nanoscale can be explained by the capacity of the different techniques used to detect changes at an early stage. From the results at 22 °C, where only β'-2 and β-2 phases are formed and there is no α-2 formation, we can confirm that microscopy allows an earlier detection of a structural transition than XRD and NMR. At 22 °C, we visualized the formation of individual elements in the microscopy images already in region II, but we only detected changes in the nanostructure (XRD), G′ and SFC in region III. We thus concluded that a paired microscale and nanoscale transition was detected at an earlier stage using microscopy than using XRD.

The rheological changes in regions II and III correspond to two stages of the same multiscale transition, which can be detected when it starts (region II) with microscopy and when it accelerates (region III) with XRD and NMR. In region II, at all temperatures, β'_1-

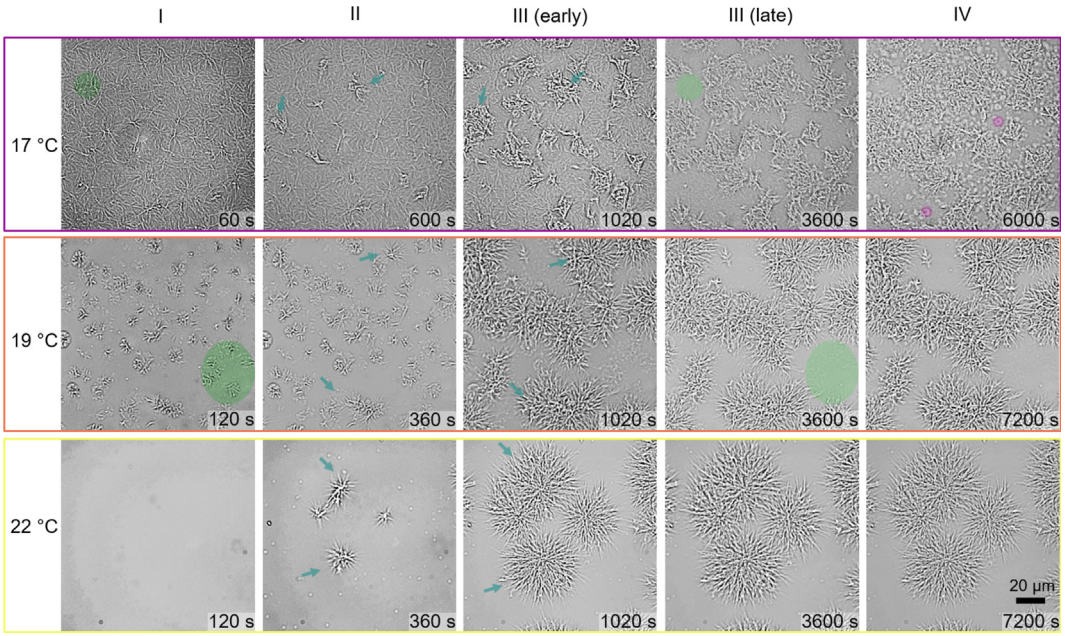

Fig. 6. Changes in the microstructure observed at representative temperatures in four time regions (I-IV). At the beginning of the crystallization (I), the first elements (green circles) form. Prior to the detection of a polymorphic transition by XRD, a new type of element (blue arrows) forms (II). At the beginning of the polymorphic transition, those new elements grow (III early). After the polymorphic transition, the first elements have disappeared as indicated by the green circles (III late). At 17 °C, a third type of element (pink circles) appears in region IV. At 22 °C, only one type of element (blue arrows) forms (II) and grows (III early).

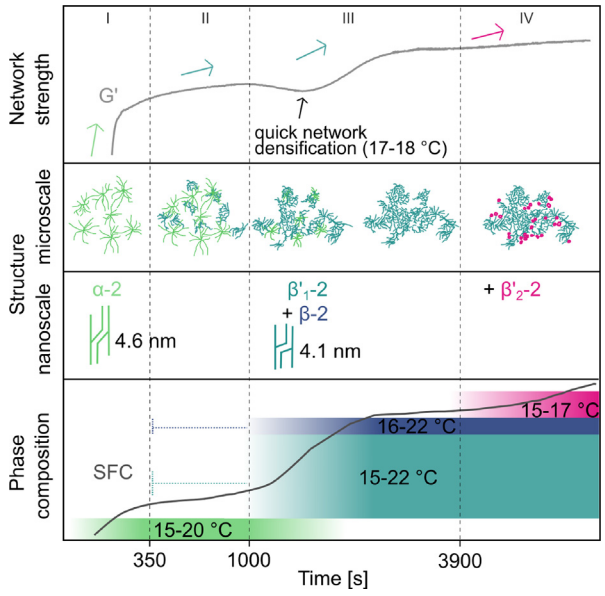

Fig. 7. Changes in the storage modulus (G′) and the solid fat content (SFC) in crystallizing milk fat are linked by synchronized structural transitions in different length scales. The transitions observed depend on the crystallization temperature and occurred in four time regions (I-IV). The microscopic elements that appear in region II are presumably formed by β'_1-2 and β-2, although these polymorphs are first detected in region III. The time scale was altered for illustration purposes.

2 crystallites appear and form new microscopic elements. At temperatures where a crystalline network was already formed in region I, the structural change in region II is also reflected as a G′ increment. This was especially clear at 18 °C, for which the G′ increment was most pronounced. The weak network formed in region I at 18 °C was considerably reinforced with new contact points that were obtained due to the microstructural change. At lower temperatures, the structural change had a limited effect on G′, as the preexisting network was already strong due to a higher SFC. For higher temperatures, i.e. 19–22 °C, no effects were observed in G′ in region II, as the limited SFC prevented the formation of a network, even after the formation of the new structural elements. The beginning of the multiscale transition was thus detected with rheology only when a network had already formed in region I.

In region III, synchronized with SFC and G′ increments and the detection and growth of the β'-2 polymorph, we observed the fast growth of the microscopic elements that were formed in region II. At 16-22 °C, ~1% of β-2 polymorph formed together with the predominant β'-2 phase, but no separate microscopic elements could be attributed to it. At 15–20 °C, we also observed the disappearance of the α-2 microstructures that were formed in region I. Thus, region III corresponds to the accelerated growth of β'-2, at the expense of the α-2 structures and the liquid. At temperatures at which limited or no α-2 structures were present (19–22 °C), the growth of the β'-2 structures finally resulted in the formation of a 3D crystal network, explaining the 1-step G′ increment observed. At lower temperatures, where the network of the α-2 structures was already sufficient to provide a G′ increase, the growth of the β'-2 structures densified the existing network, which was reflected as G′ increments at 15 °C and 16 °C. At 17 °C and 18 °C, this densification also produced steep G′ increments, but prior to that, we observed a temporary decline in G′ at 17 °C and a plateau at 18 °C, even though the SFC increased. This decline can thus not be explained by the volume fraction of the crystallites making up the network, but by the densification of the crystallites. At 17 °C and 18 °C, we indeed observed the fastest densification (Fig. 1c and d), as the lamellar thickness decreased from ~4.7 nm lamellae to ~4.1 nm, when the α-2 polymorphs transitioned to the $\beta\prime$-2 and β-2 polymorphs. Such quick densification of the crystallites led to a decrease in the crystal volume fraction, while still increasing the SFC, which resulted in a temporary loss of inter- and intra-particle links within the network. Once the volume fraction of crystalline matter increased again due to crystal growth, the network was restored, and G′ increased again. Thus, densification would only visibly decrease G′ at temperatures at which the transition

is so fast that its effect cannot immediately be compensated by crystal growth.

In region IV, coinciding with the SFC increments at temperatures below 19 °C, a third type of microscopic element formed on the edges of the crystal networks. As indicated by XRD patterns, these elements were composed of a second β'-2 phase (β'_2-2), as both structures appeared at the same time. At 18 °C, we observed fewer and smaller elements forming in this period, which would explain why we did not detect them in the rheogram or the XRD patterns. Overall, we see that the used techniques are complementary, and provide a clear picture of how initial crystal growth at different temperatures can be related to specific polymorphic transitions, microstructural development, and final macroscopic properties of the system.

4. Conclusions

Our aim was to study the effect of temperature on the isothermal crystallization of MF, linking the network formation to changes in multiscale structures, with a special focus on polymorphism. We hypothesized that rheology could be used to monitor those multiscale transitions, as the network strength would increase due to changes in the microstructure, paired with changes in the lateral and the longitudinal arrangement of TAGs. Although XRD and NMR were needed to quantify the phase transitions, microscopy proved to be better in identifying the beginning of such transitions. Rheology was also found to be an effective technique to monitor the whole crystallization process, as the G′ reflected the changes observed with the other techniques, including the beginning of the multiscale transition observed with microscopy. However, it is important to bear in mind that rheological changes were only observed in the presence of a 3D crystal network, as changes in individual particles did not affect the G′. The fact that rheology and microscopy could reflect the structural transitions earlier than XRD and NMR also shows that, in crystallization studies, differences in sample size and heat transfer have a minor effect in comparison with the detection limits of the different techniques.

Although the formation of β'_1-2 is often reported in literature [8,10,13], our study advances the current knowledge by quantifying the simultaneous formation of β'_1-2, and the delayed formation of the low-melting β'_2-2 polymorph. β'_2-2 could only be quantified using WAXD, displaying the advantage of the new approach we previously proposed [9]. The formation of a β'_2-2 polymorph in MF has rarely been reported and has only been observed after long storage periods at a much lower temperature (4 °C) [4,5]. For the first time, we have observed and quantified the formation of the β'_2-2 polymorph in MF at an early crystallization stage.

We propose two hypotheses that explain the limited β-2 formation and its erratic observation in MF studies: (1) there is a small amount (~1%) of β-tending TAGs in MF and (2) β can only form at an early crystallization stage in a specific temperature range in which there is a balance between a low kinetic constraint (low viscosity) and a sufficient degree of supercooling for the β-tending TAGs. These hypotheses are supported by our results and those presented in previous studies [9,18,23]. We recommend further research to verify our novel findings: the crystallization of specific β-tending TAGs within a narrow temperature range, the delayed crystallization of a second β'-2 phase (β'_2-2) and the ability to detect polymorphic transitions at an earlier stage using rheology and microscopy.

CRediT authorship contribution statement

Naomi Arita-Merino: Conceptualization, Formal analysis, Visualization, Funding acquisition, Investigation, Methodology, Writing – original draft, Writing – review & editing. **Laura te Nijenhuis:** Visualization, Investigation, Writing – review & editing. **Hein van Valenberg:** Conceptualization, Funding acquisition, Writing – review & editing, Supervision, Resources. **Elke Scholten:** Conceptualization, Funding acquisition, Writing – review & editing, Supervision.

Declaration of Competing Interest

The authors declare that they have no known competing financial interests or personal relationships that could have appeared to influence the work reported in this paper.

Acknowledgements

We thank FrieslandCampina for providing access to the AMF sample and the NMR equipment, and especially Jeroen van Binsbergen for his technical support. We acknowledge the European Synchrotron Radiation Facility for provision of synchrotron radiation facilities and we would like to thank Daniel Hermida Merino for assistance in using beamline BM26B.

This work was supported by the Consejo Nacional de Ciencia y Tecnologia (grant number 474601).

Appendix A. Supplementary material

Supplementary data associated with this article can be found, in the online version, at https://doi.org/10.1016/j.jcis.2021.09.071.

References

[1] A.G. Marangoni, J.P.M. van Duynhoven, N.C. Acevedo, R.A. Nicholson, A.R. Patel, Advances in our understanding of the structure and functionality of edible fats and fat mimetics, Soft Matter. 16 (2020) 289–306.
[2] Z. Liu, C. Li, J. Pryce, S. Rochfort, Comprehensive Characterization of Bovine Milk Lipids: Triglycerides, ACS Omega. 5 (2020) 12573–12582.
[3] R.E. Timms, The phase behaviour and polymorphism of milk fat, milk fat fractions and fully hardened milk fat, Aust. J. Dairy Technol. TA - TT -. 35 (1980) 47–53.
[4] C. Lopez, P. Lesieur, C. Bourgaux, M. Ollivon, Thermal and Structural Behavior of Anhydrous Milk Fat. 3. Influence of Cooling Rate, J. Dairy Sci. 88 (2005) 511–526.
[5] C. Lopez, C. Bourgaux, P. Lesieur, M. Ollivon, Crystalline structures formed in cream and anhydrous milk fat at 4 °C, Lait. 82 (2002) 317–335.
[6] S. Bugeat, J. Perez, V. Briard-Bion, P. Pradel, A. Ferlay, C. Bourgaux, et al., Unsaturated fatty acid enriched vs. control milk triacylglycerols: Solid and liquid TAG phases examined by synchrotron radiation X-ray diffraction coupled with DSC, Food Res. Int. 67 (2015) 91–101.
[7] R.E. Timms, Phase behaviour of fats and their mixtures, Prog. Lipid Res. 23 (1984) 1–38.
[8] E. ten Grotenhuis, G.A. van Aken, K.F. van Malssen, H. Schenk, Polymorphism of milk fat studied by differential scanning calorimetry and real-time X-ray powder diffraction, J. Am. Oil Chem. Soc. 76 (1999) 1031–1039.
[9] N. Arita-Merino, H. van Valenberg, E.P. Gilbert, E. Scholten, Quantitative Phase Analysis of Complex Fats during Crystallization, Cryst. Growth Des. 20 (2020) 5193–5202.
[10] M.L. Herrera, M. de León Gatti, R.W. Hartel, A kinetic analysis of crystallization of a milk fat model system, Food Res. Int. 32 (1999) 289–298.
[11] J. Toro-Vazquez, V. Herrera-Coronado, E. Dibildox-Alvarado, M. Charo-Alonso, C. Gomez-Aldapa, Induction Time of Crystallization in Vegetable Oils, Comparative Measurements by Differential Scanning Calorimetry and Diffusive Light Scattering, J. Food Sci. 67 (2002) 1057–1064.
[12] V. de Graef, K. Dewettinck, D. Verbeken, I. Foubert, Rheological behavior of crystallizing palm oil, Eur. J. Lipid Sci. Technol. 108 (2006) 864–870.
[13] L. Wiking, V. de Graef, M. Rasmussen, K. Dewettinck, Relations between crystallisation mechanisms and microstructure of milk fat, Int. Dairy J. 19 (2009) 424–430.
[14] S. Yener, H.J.F. van Valenberg, Characterisation of triacylglycerols from bovine milk fat fractions with MALDI-TOF-MS fragmentation, Talanta. 204 (2019) 533–541.
[15] AOCS, AOCS Official Method Cd 16b-93 Solid Fat Content (SFC) by Low-Resolution Nuclear Magnetic Resonance, Direct Method, (2017).
[16] K. Larsson, S.J. Cyvin, L. Rymo, J.H. Bowie, D.H. Williams, E. Bunnenberg, et al., Classification of Glyceride Crystal Forms, Acta Chem. Scand. 20 (1966) 2255–2260.

[17] E. Fredrick, D. van de Walle, P. Walstra, J.H.H. Zijtveld, S. Fischer, P. van der Meeren, et al., Isothermal crystallization behaviour of milk fat in bulk and emulsified state, Int. Dairy J. 21 (2011) 685–695.
[18] G. Mazzanti, S.E. Guthrie, E.B. Sirota, A.G. Marangoni, S.H.J.J. Idziak, Effect of minor components and temperature profiles on polymorphism in milk fat, Cryst. Growth Des. 4 (2004) 1303–1309.
[19] C. Lopez, F. Lavigne, P. Lesieur, G. Keller, M. Ollivon, Thermal and Structural Behavior of Anhydrous Milk Fat. 2. Crystalline Forms Obtained by Slow Cooling, J. Dairy Sci. 84 (2001) 2402–2412.
[20] S. Pacheco-Pappenheim, S. Yener, J.M.L. Heck, J. Dijkstra, H.J.F. van Valenberg, Seasonal variation in fatty acid and triacylglycerol composition of bovine milk fat, J. Dairy Sci. (2021).
[21] A. Cisneros, G. Mazzanti, R. Campos, A.G. Marangoni, Polymorphic Transformation in Mixtures of High- and Low-Melting Fractions of Milk Fat, J. Agric. Food Chem. 54 (2006) 6030–6033.
[22] A. Marangoni, L. Wesdorp, Crystallography and Polymorphism, in: Struct. Prop. Fat Cryst. Networks, 2nd ed., CRC Press, Boca Raton, 2012, pp. 19–44.
[23] D.A. Tzompa-Sosa, P.R. Ramel, H.J.F. van Valenberg, G.A. van Aken, Formation of β Polymorphs in Milk Fats with Large Differences in Triacylglycerol Profiles, J. Agric. Food Chem. 64 (2016) 4152–4157.
[24] P.R.R. Ramel, F. Peyronel, A.G. Marangoni, Characterization of the nanoscale structure of milk fat, Food Chem. 203 (2016) 224–230.